Received: 22 December 2019 | Revised: 30 September 2020 | Accepted: 8 October 2020

IET Renewable Power Generation

DOI: 10.1049/rpg2.12061

The Institution of Engineering and Technology WILEY

ORIGINAL RESEARCH PAPER

Cascade-I$^{\lambda}$D$^{\mu}$N controller design for AGC of thermal and hydro-thermal power systems integrated with renewable energy sources

Yogendra Arya[1] | Nishant Kumar[2] | Pankaj Dahiya[3] | Gulshan Sharma[4] | Emre Çelik[5] | Sandeep Dhundhara[6] | Mandeep Sharma[7]

[1] Department of Electrical and Electronics Engineering, Maharaja Surajmal Institute of Technology, Janakpuri, New Delhi, India

[2] Electrical and Computer Engineering Department, Postdoctoral Research Fellow, National University of Singapore, Singapore

[3] Department of Electronics & Communication Engineering, Delhi Technological University, Shahbad Daulatpur Village, Rohini, Delhi, India

[4] Department of Electrical Power Engineering, Durban University of Technology, Durban, South Africa

[5] Department of Electrical and Electronics Engineering, Engineering Faculty, Düzce University, Düzce, Turkey

[6] Department of Basic Engineering, College of Agricultural Engineering and Technology, CCS Haryana Agricultural University, Hisar, India

[7] Department of Electrical Engineering, Baba Hira Singh Bhattal Institute of Engineering and Technology, Lehragaga, Punjab, India

Correspondence
Yogendra Arya, Department of Electrical and Electronics Engineering, Maharaja Surajmal Institute of Technology, Janakpuri, New Delhi, India.
Email: mr.y.arya@gmail.com

Abstract

Expert, intelligent and robust automatic generation control (AGC) scheme is requisite for stable operation and control of power system (PS) integrated with renewable energy sources (RES) under sudden/random small load disturbances. Large frequency deviations appear if AGC capacity is inept to compensate for the imbalances of generation and demand. In this paper, a cascade-fractional order ID with filter (C-I$^{\lambda}$D$^{\mu}$N) controller is proposed as an expert supplementary controller to promote AGC recital adequately in electric power systems incorporated with RES like solar, wind and fuel cells. The imperialist competitive algorithm is fruitfully exploited for optimizing the controller parameters. First, a 2-area reheat thermal system is examined critically and then to authorize the worth of the proposed controller, the study is protracted to a 2-area multi-source hydro-thermal system. The prominent benefits of C-I$^{\lambda}$D$^{\mu}$N controller with/without renewable energy sources consist of its great indolence to large load disturbances and superiority over various optimized classical/fuzzy controllers published recently. The sensitivity study validates the robustness of the recommended controller against ±20% deviations in the system parameters and random step load perturbations.

1 | INTRODUCTION

The generation control is progressively turning challenging due to the gradual enhancement in the power demands and depletion of power resources. The expanding power demands are posing severe dangers to the stable conduct of power system. The growing power demand causes sluggishness in turbine speed and hence, frequency in output voltage of the alternator decline undesirably. In an interconnected large-scale power system (PS), all the synchronously connected generation units perform with the common frequency. It is desirable to sustain frequency/scheduled tie power flows irrespective of load variations in control areas of interconnected PS during normal operating and small abrupt disturbance conditions. To carry out this, an efficient and intelligent automatic generation control (AGC) strategy is vital to spontaneously manipulate the operation of hydro or steam valves which regulates real output power of generators [1].

The PS is turning complicated day-by-day, because of upsurge in its dimension and mixing of renewable energy sources (RES). Because of the ongoing depletion of fossil fuels and the environmental hazards caused by them, the

This is an open access article under the terms of the Creative Commons Attribution License, which permits use, distribution and reproduction in any medium, provided the original work is properly cited.
© 2021 The Authors. *IET Renewable Power Generation* published by John Wiley & Sons Ltd on behalf of The Institution of Engineering and Technology

infiltration of RES in modern power system is attracting electricity industry. The fascinating features of RES are that they are environmentally-friendly and ample in nature. Furthermore, due to the advancement in technology and bulk production, their energy conversion efficiency is swelling and the cost is shrinking year by year [2]. However, the RES such as solar and wind are extensively accessible in nature and dominate other RES. Hence, the penetration of wind and solar into the prevailing power systems has constantly been a prominent area of curiosity for researchers. Rahman et al. studied the impact of a dish-Stirling solar thermal system in AGC of a 2-area reheat thermal system (RTS) [2]. Kler et al. conducted an AGC study on a 2-area RTS having RES like wind turbine generators (WTGs), solar thermal generators (STGs) and aqua electrolyser (AE)-fuel cells (FCs) units [3]. An independent hybrid generating system comprising of WTG, STG, solar photovoltaic (PV), diesel engine generators, AE, FC, battery energy storage system (BESS), flywheel energy storage system and ultracapacitors is studied comprehensively in [4]. The recent literature presented a critical study on the impact of AE-FC units on AGC performance of interconnected 2-area non-reheat thermal system, PV-reheat thermal and multi-source hydro-thermal system (MSHTS) [5]. Further, the effects of STG and geo thermal (GT) plants are recently inspected in 2 and 3-area deregulated systems [6, 7]. An islanding smart distribution network heavily penetrated with renewable sources is demonstrated in [8]. Hubei power grid composed of thermal, pumped storage, hydro and distributed renewable energy sources (DREs) is inspected in [9]. Guangdong power grid having thermal, hydro, wind, PV and electric vehicles is studied in [10]. A 3-area micro grid system having various DREs is proposed in [11]. Consequently, various RES systems are studied in different AGC system. But, there still exists scope for AGC of interconnected power systems with integration of RES such as STGs, WTGs and AE-FC units. This necessities additional examination as tried here.

The competence of an AGC system is stated in terms of brisk and stress-free control action. With the integration of RES, power system requires robust and efficient AGC strategy to withstand its controllability and stability in the presence of stochastic nature of RES. To boost AGC outcome, different control and tuning approaches are available in the recent literature. Some of them implemented in various traditional and restructured systems are classical [1], minority-charge carrier inspired algorithm optimized I/PI/ID [1], biogeography based optimisation based 3-degree-of-freedom-PID (3DOF-PID) [2], genetic algorithm (GA) based integral minus proportional derivative (IPD)/PI/PID [3, 4], imperialist competitive algorithm (ICA) based fuzzy-tilt-I-D with filter-double integral (FTIDN-II) [5], sine–cosine algorithm (SCA) tuned cascade fractional order (FO) PI-FOPIDN [6], SCA tuned cascade FOPI-FOPDN [7], wolf pack hunting strategy based control [8], multi-agent double deep Q network-action discovery (AD) based control [9], deep policy dynamics based win or learn fast-policy hill climbing (PDWoLF-PHC) network based control [10], PDWoLF-PHC(λ) strategy [11, 12], deep-reinforcement-learning-based three-network double-delay actor-critic control strategy [13], SCA optimized proportional derivative-proportional integral derivative with double derivative filter (PDPID + DDF) [14], grey wolf optimization (GWO) optimized PI/PID [15], artificial bee colony algorithm (ABCA) optimized PI/PID [16], hybrid firefly algorithm-pattern search (hFA-PS) technique optimized PI/PID [17], ICA optimized PID [18], jaya algorithm-invasive weed optimization (JA-IWO) optimized PID [19], bacterial swarm optimization (BSO) optimized PID/FOPID [20], optics inspired optimization (OIO) optimized PID [21], symbiotic organisms search (SOS) algorithm optimized PID/PIDN [22, 23], quasi-oppositional differential search algorithm (QODSA) optimized PI/PID [24], hybrid IWO-PS (hIWO-PS) tuned 2DOF-PID [25] and whale optimization algorithm (WOA) optimized cascade PIDN-FOPD [26]. Since, the operating conditions of power system are liable to vary widely over the time due to wearing out of the components, the conventional controllers optimized for fixed operating condition might work inappropriately in changed operating condition. To overcome this difficulty and to get excellent control of generation/frequency/tie power in any interconnected PS, intelligent control system like fuzzy logic controller (FLC) is recommended over conventional one [5].

FLC can handle small deviation in system operating condition efficiently by automatically adjusting the controller parameters online. With the aid of FLC, diverse intelligent conventional controllers are proposed recently [5, 27–41]. The choice of FLC parameters like input/output scaling factors (SFs), control rules (CRs), membership functions (MFs) etc. is an intricate assignment. Classically, their selection depends on operator's experiential rules and usually are non-optimal. The inappropriate assortment of FLC parameters might impact the system results adversely. Hence, to overcome this problem, various intelligent optimization methods are applied fruitfully in different types of PSs for tuning the parameters of FLC having different configurations. The procedure of concurrent optimization of all FLC parameters might be a difficult, costly and time consuming task. Hence, prevalent trend of FLC optimization is the tuning/setting of input/output SFs only and MFs/CRs are kept fixed for dissimilar models as getting their values is simpler; and also they impact the system results to a great extent [5, 27–41]. Recently, hybrid particle swarm optimization-pattern search (hPSO-PS) [27] and bacterial foraging optimization algorithm (BFOA) [28] techniques are adopted to tune input/output SFs and ICA [29] to tune output SFs of fuzzy PI (FPI) controller. But, FPI structure may probably show substandard performance due to its inherent integral action. To conquer this drawback, a derivative mode is attached in PI configuration to get FPID structured controller. To improve FPI performance, some researchers have implemented different optimization methods to tune FPID controller. BFOA [28]/hybrid PSO-levy flight algorithm (hPSO-LFA) [30]/hybrid harmony search-cuckoo optimization algorithm (hHS-COA) [31]/hybrid improved FA-PS (hIFA-PS) [32] and hybrid differential evolution-PSO (hDE-PSO) [33] are employed efficiently to tune input/output SFs of FPID controller for different types of systems. In FPID controller, since derivative block is affected by higher frequency noise in area control error (ACE) fed to FPID, a first order filter is employed in derivative block to

attenuate higher frequency noise to get FPID with filter (FPIDN) controller. In the literature, some researchers have employed FPIDN controller with input/output SFs selected using hybrid local unimodal sampling-teaching learning based optimization (hLUS-TLBO) [34]/jaya algorithm (JA) [35] algorithm and it shows better performance than FPID controller.

Fractional order (FO) controllers are earning fame in the current years due to their extra flexibility and skill to handle control design specifications. FO controllers are verified to be superior than their integer order (IO) equivalents [36–41]. Recently, FO controllers are implemented in PS models and desirable results are observed. Further, the literature review indicates that the hybridization of fuzzy controller with FO controller shows enhanced performance compared to fuzzy hybridized with conventional controller. A FO fuzzy PID (FOFPID) controller tuned recently using ICA [36], BFOA [37, 38] and quasi-oppositional harmony search algorithm (QOHSA) [39] displays healthier results compared to their conventional counterparts for different single/multi-area PSs. Further, some intelligent cascade controllers like SCA based FOPI-FOPID [6]/FOPI-FOPD [7], WOA optimized PIDN-FOPD [26] and ICA based FFOPI-FOPD [40]/FOPID [41] are appeared in the literature. However, the performance assessment of cascade fuzzy-FOIDN (C-I$^{\lambda}$D$^{\mu}$N) structured controller has not been explored so far. Considering these facts, a C-I$^{\lambda}$D$^{\mu}$N controller is recommended for 2-area PS models. Besides the controller construction, system performance also relies on the suitable choice of optimization technique to tune the controller parameters. Due to better convergence rate, scarcity in AGC applications, robust control performance of ICA against nonlinearities, constraints and parameters uncertainties, the optimal adjustment of C-I$^{\lambda}$D$^{\mu}$N controller parameters is attained by adopting ICA.

Considering the above analysis, the novel contributions of this work are stated as follows:

(i) To propose a novel ICA tuned C-I$^{\lambda}$D$^{\mu}$N structured controller for AGC of interconnected 2-area RES penetrated RTS and MSHTS.
(ii) To authenticate the strength of the proposed method compared to the various intelligent control strategies existing in the state-of-the-art literature.
(iii) To exemplify the returns of RES penetration in RTS and MSHTS.

1.1 | Power system models

The AGC models investigated are 2-area RTS displayed in Figure 5(a) [3, 16, 20, 22, 28, 33] and 2-area MSHTS displayed in Figure 8 [15, 17, 28, 29, 34]. The systems consist of generating areas of equal sizes. The RTS consists of one single reheat type of turbine and MSHTS comprises of one non-reheat and one hydro turbines in each area. Both systems in area-1 embrace renewable energy sources (RES) based systems involving of 2 solar thermal generators (STGs), 3 wind turbine generators (WTGs), 1 aqua-electrolyser (AE) and 2 fuel cells (FCs). As this study is conducted in low frequency domain, the transfer functions (TFs) for these RES are denoted by first order lag [2–5]. The STG entails solar and thermal parts. The solar part comprises of parabolic collectors which targets the sunlight on to the thermal part to generate steam to run the turbine [3]. The AE is exploited to engage portion of the inconstant power produced by STGs and WTGs to generate hydrogen [3, 5]. Analogous to STGs and WTGs, the FC is also characterized via first order lag-based TF having time constant obtained experimentally [3]. The detailed RES system is demonstrated in Figure 5(b) [3].

Every control area comprises its own speed governing system, turbine and generator. There are three inputs and two outputs for an area. The inputs are control input that is, ΔP_C, change in load demand that is, ΔP_D, and change in tie power that is, ΔPtie. One extra input in area-1 exists due to RES output that is, ΔP_{gRES}. The outputs consist of change in area frequency (ΔF) and area control error (ACE). The test models are picked up from the literature stated above. The data used for the systems have been taken from the stated references and given in Appendix. The Nomenclature describes various symbols used.

2 | CONTROLLER STRUCTURE

The major intentions of a controller designed for an AGC system are to force frequency, generation and tie power variations to zero with least over/under shoots as swiftly as possible under sudden/step load perturbation (SLP). Under SLP, the resultant area control error (ACE) is employed to call upon the controller action to curtail ACE to zero in possible minimum time in each area. Conventional PID controller is favoured in the majority of PS industry due its simple design, robust performance, inexpensive and effective potential for use in the engineering disciplines. Though, because of the inherent intricacy of the extended PS, presence of nonlinearities, uncertainties and their combined impacts, PID controllers become comparably ineffectual to provide a desired level of resilience and outcome in changing operating situations of large scale PS. On the other hand, PID with fuzzy logic (FL) has demonstrated better flexibility and performance to achieve the challenges in PS control. The FL combined with PI/PID/PIDN/FOPID controller is recommended in majority of the recently appeared AGC literature [5, 27–41]. But, cascade type of fuzzy controller has not been discussed more. Hence, in this paper, a cascade fuzzy FOIDN (C-I$^{\lambda}$D$^{\mu}$N) controller is recommended for AGC of multi-area PSs as an expert, robust and intelligent controller. The controller construction is exposed in Figure 1. It consists of a FPIDN and I$^{\lambda}$D$^{\mu}$N controllers connected in cascade. The FPIDN has area control area (ACE) and derivative of ACE as two inputs. The area-1 (ACE$_1$) and area-2 (ACE$_2$) ACEs are given by

$$\left.\begin{aligned} \mathrm{ACE}_1 &= B_1 \Delta F_1 + \Delta P\mathrm{tie}_{12} \\ \mathrm{ACE}_2 &= B_2 \Delta F_2 + \alpha_{12} \Delta P\mathrm{tie}_{12} \end{aligned}\right\} \quad (1)$$

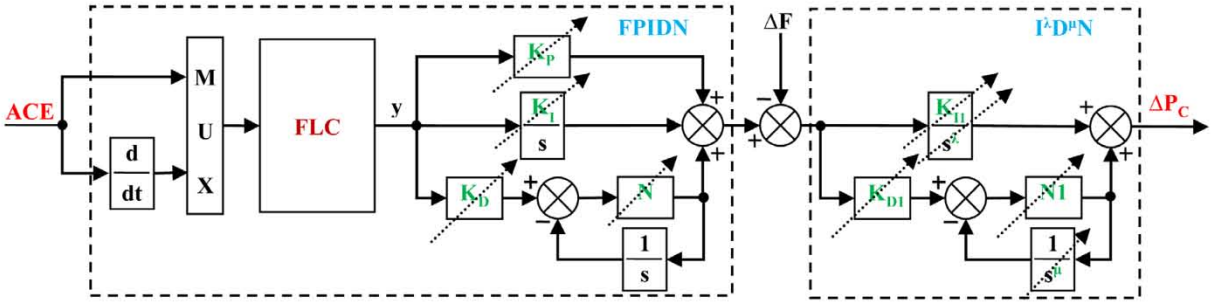

FIGURE 1 Configuration of C-$I^\lambda D^\mu N$ controller

where, B_i is the frequency bias, ΔF_i is area frequency deviation, $\Delta P\text{tie}_{ij}$ is tie flow deviation, α_{12} is the control area rating ratio. The FLC output y performances as the input to PIDN controller. The output of C-$I^\lambda D^\mu N$ controller is the control input ΔP_C for the PS as represented by Equation (2).

$$\Delta P_C = \left[\left\{\left(yK_p + \frac{yK_I}{s} + \frac{ysNK_D}{s+N}\right) - \Delta F\right\} \times \left(\frac{K_{I1}}{s^\lambda} + \frac{s^\mu N1 K_{D1}}{s^\mu + N1}\right)\right] \tag{2}$$

Fractional calculus (FC) is expansion of the nth order continuous differentiation/integration of an arbitrary function with a real value order. The notions of FO controller connect with differential equations employing FC. The FOPID/FOPIDN controller is the expansion of the integer order (IO) PID/PIDN controller with fractional choice of integral-differential orders along with the IO PID/PIDN controller gains. The transfer function (TF) portrayal of FOPID ($PI^\lambda D^\mu$)/FOIDN ($I^\lambda D^\mu N$) controller is given as:

$$C(s) = K_P + \frac{K_I}{s^\lambda} + K_D s^\mu \ (PI^\lambda D^\mu) \tag{3}$$

$$C(s) = \frac{K_{I1}}{s^\lambda} + \frac{K_{D1} s^\mu N1}{s^\mu + N1} \ (I^\lambda D^\mu N) \tag{4}$$

In Equations (2) and (4), N and $N1$ denote coefficients of filter. The $N/N1$ curtails the impact of high frequency noise that appears because of regular switching of loads. In this work a well-known approximation termed as CRONE approximation, proposed by Oustaloup is utilized [6]. CRONE practices a recursive dispersal of A poles and A zeros leading to a TF inside a pre-specified frequency limit [ω_L, ω_H]. For computer simulations, the considered ω_L, ω_H and A are 0.01 rad/s, 100 rad/s and 6, in order. For further details of FO controllers, [6, 7, 20, 26, 36–41] can be referred.

The controller gains of C-$I^\lambda D^\mu N$ controller are to be selected via an appropriate method. Here, seven membership functions (MFs) are adopted for each inputs/output. The innermost five MFs have triangular shapes and the outer two have trapezoidal shapes as showcased in Figure 2 [29]. The rule base is utilized from [29]. In Figure 2, the fuzzy linguistic variables L, N, M, S, Z and P signify large, negative, medium, small, zero and positive, in order. The unfuzzified output of FLC is decided via center of gravity defuzzification method and rule base is fired adopting Mamdani fuzzy inference system (FIS).

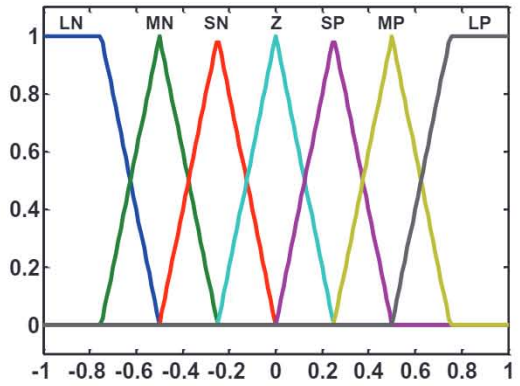

FIGURE 2 MFs for FLC inputs/output [29]

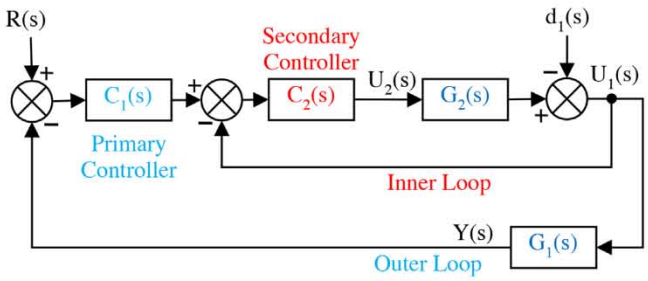

FIGURE 3 Cascade controller model

Handling two subsequent processes gives the notion of cascade control (CC). CC can advance control system outcome compared to single-loop control. CC is effective in fast disturbance rejection and provides fast/enhanced system response [6, 41]. The basic CC system includes two control loops as revealed in Figure 3. In Figure 3, primary/master/outer controller $C_1(s)$ is FPIDN and secondary/slave/inner controller $C_2(s)$ is FOIDN. The primary process is termed as $G_1(s)$ and the complete process is exposed to load disturbance $d_1(s)$ creating $Y(s)$ output. The input to $G_1(s)$ is $U_1(s)$, which is the inner process output. $Y(s)$ is organized in reference to $R(s)$. $U_2(s)$ is the input to the secondary loop process $G_2(s)$. The

major purpose of the secondary loop is to bound the result of secondary process gain deviations on the control system outcome [6, 7]. These gain changes might originate from variations in operating conditions.

3 | IMPERIALIST COMPETITIVE ALGORITHM (ICA)

ICA, a meta-heuristic evolutionary algorithm stimulated by socio-political practices of imperialistic competition of people in the physical world was established by Atashpaz–Gargari and Lucas [42]. It establishes abundant recital both in convergence rate and global optimal solution achievement. It commences with early population of countries segregated into two groups; imperialists having the best/lowest values of fitness/cost function and other countries with less power named as colonies of the imperialists and all together constitute few initial empires. In the initial population, the colonies attached with the imperialists based on imperialists' powers so that the imperialist with extra power has extra colonies. The empire's power depends on the powers of the imperialist and its colonies. The colonies begin to vary their societies as per relevant imperialist. Here, colonies start moving regarding their relevant imperialist and this process is called assimilation. In it, the colony having more power may swap the imperialist with less power and vice versa.

During the imperialistic competition among the empires; the powerful empires try to boost their powers. The empires which are not powerful enough to compete and not able to raise their power will crumble. The competition will slightly enhance the power of powerful empires and decrease the power of less-powerful empires. Due to this, during imperialistic competition, feeble empires will gradually lose their powers and breakdown at last. At the completion of competition, countries converge to a condition where there exists only one empire, all countries act as colonies of this empire and these colonies occupy the equivalent position/power as the imperialist.

The main steps concerned with the decision regarding the optimal controller parameters via ICA are specified as follows.

3.1 | Initialize the empires

In this step, an array of variables (country) to be optimized is decided as:

$$\text{Country} = \left[p_1, p_2, p_3, \ldots, p_{\text{n}}\right], n = 1, 2, \ldots, N_{\text{var}} \tag{5}$$

where, p_i are variables to be tuned. The country's cost is determined as:

$$\text{cost} = \text{f}\left(\text{country}\right) = \text{f}(p_1, p_2, p_3, \ldots, p_n) \tag{6}$$

To shape the early empires, the colonies are distributed among imperialist evenly using the imperialist's normalized cost

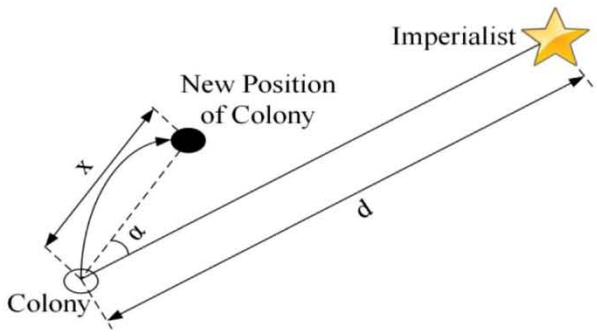

FIGURE 4 Shifting of a colony to its related imperialist [37]

described as:

$$\text{C}_n = \text{C}_n - \max_i \left(\text{C}_i\right) \tag{7}$$

here, C_n is the nth imperialist's cost and C_n denotes its normalized cost. The normalized power of each imperialist is obtained as:

$$P_n = \frac{|\text{C}_n|}{\left|\sum_{i=1}^{N_{\text{imp}}} \text{C}_i\right|} \tag{8}$$

here, N_{imp} denotes the powerful countries to be imperialists to constitute empires. The nth empire's colonies can be given as:

$$N \times \text{C}_n = \text{round}(P_n \times N_{\text{col}}) \tag{9}$$

here, $N \times \text{C}_\text{n}$ denotes nth empire's preliminary colonies and N_{col} is the total number of colonies.

3.2 | Assimilation

The colonies of every imperialist are assimilated regarding their particular imperialist as:

$$x_{\text{col}}^{\text{new}} = x_{\text{col}}^{\text{old}} + \beta \times x \otimes \left(x_{\text{imp}} - x_{\text{col}}^{\text{old}}\right) \tag{10}$$

here, $x_{\text{col}}^{\text{old}}$ depicts colony's old position, β denotes assimilation factor and x is a random variable with even distribution. X_{imp}, $X_{\text{col}}^{\text{new}}$ are the imperialist's position and colony's new position, in order. Figure 4 displays the drive of a colony near its related imperialist. The progress is explained via x (distance) and α (angle) chosen randomly with even distribution (11-12).

$$x = \text{u}(0, \beta \times \text{d}) \tag{11}$$

$$\alpha = u\left(-\eta, \eta\right) \tag{12}$$

where $\beta > 1$, d denotes the distance between colony-imperialist and η is a limit angle for adjusting departure from the original direction [42].

TABLE 1 Optimized gains of controllers

	2-area reheat thermal system		2-area multi-source hydro-thermal system		
Controller gains	C-I$^{\lambda}$D$^{\mu}$N	C-I$^{\lambda}$D$^{\mu}$N (RES)	FPIDN	C-I$^{\lambda}$D$^{\mu}$N	C-I$^{\lambda}$D$^{\mu}$N (RES)
K_P	4.3654	4.8625	2.3021	2.3645	2.8599
K_I	9.5127	9.3283	7.8988	4.6854	5.9901
K_D	0.1354	0.2531	0.0894	0.1354	0.1845
N	482.3548	397.2634	250.2364	409.6856	395.8695
K_{I1}	7.3524	9.9289	–	4.3655	5.9649
λ	0.3395	0.2595	–	0.5528	0.5027
K_{D1}	0.5920	0.8121	–	0.8369	0.8082
μ	0.3843	0.3495	–	0.0525	0.0687
$N1$	468.9861	406.4528	–	463.6857	426.5469

3.3 | Switching positions

During drive in the direction of the imperialist, a colony may arrive at a station having lesser cost value compared to the imperialist. In this case, the position of imperialist and colony are interchanged and then colonies commence moving near this new location.

3.4 | Total cost of empires

An empire comprises of the imperialists and colonies. Hence, the cost of an empire is given as:

$$T \times \mathrm{C}_n = \mathrm{f}(\text{imperialist}_n) + \xi \times \text{mean}(\{\mathrm{f}(\text{colonies of empires}_n)\} \tag{13}$$

here, $T \times C_n$ is the nth empire's total cost and ξ is a positive number < 1. A small value of ξ implies that the empire's power is due to only the imperialist. However, a high value of ξ implies that the empire's total power is due to mainly the colonies.

3.5 | Imperialist competition

In imperialist competition (IC), the power of frailer empires gradually decreases and that of powerful ones increases. This practice embraces the competition between imperialists to snatch colonies associated with other imperialists and this is performed by choosing the weakest colony from the weakest empire and creating a competition among all empires to own this colony. The most dominant empire conquers the selected colony. To initialize the IC, primary, the possession probability (PP) of every empire is calculated on the basis of its total power. The normalized cost of nth empire is computed by

$$NT \times \mathrm{C}_n = T \times \mathrm{C}_n - \max_i (T \times \mathrm{C}_i) \tag{14}$$

here $NT \times C_n$ is the nth empire's normalized cost. The PP of every empire is calculated as:

$$P_{\mathrm{pn}} = \frac{|NT \times \mathrm{C}_n|}{\left|\sum_{i=1}^{N_{\mathrm{imp}}} NTC_i\right|} \tag{15}$$

After computing the PP vector, additional vector termed D having the equal size is expressed by subtracting R (a random vector) from the PP vector ($D = P - R$), the possessed colony owns the highest value of D.

3.6 | Revolution

In each iteration, in addition to assimilation, the revolution process is utilized to shift the colony positions. Few weakest colonies are selected and replaced with new colonies, haphazardly. Revolution is a sudden change, which improves the exploitation and exploration processes. It creates variety during searching of solution space. Comparable to the mutation process in GA, revolution advances the global convergence and thwart ICA from being trapped in local minimum. The number of colonies presumed to be interchanged with the equal number of new colonies is:

$$N_{\mathrm{RC}} = \text{round}\{\mathrm{P}_{\text{revolution}} \times \text{No.(colonies of empire}_n)\} \tag{16}$$

here N_{RC} denotes revolutionary colonies and $P_{\text{revolution}}$ is the revolution rate. Prior the movement of each colony, a random number having constant distribution [0,1] is originated and matched with $P_{\text{revolution}}$. If this number is less than $P_{\text{revolution}}$, revolution process is adopted and the recent colony will substitute with the previous one.

3.7 | Eliminating powerless empires

In the imperialist competition, feeble empires will breakdown and colonies associated with them will be allocated among remaining empires. An empire is expected to downfall when it drops all of its colonies.

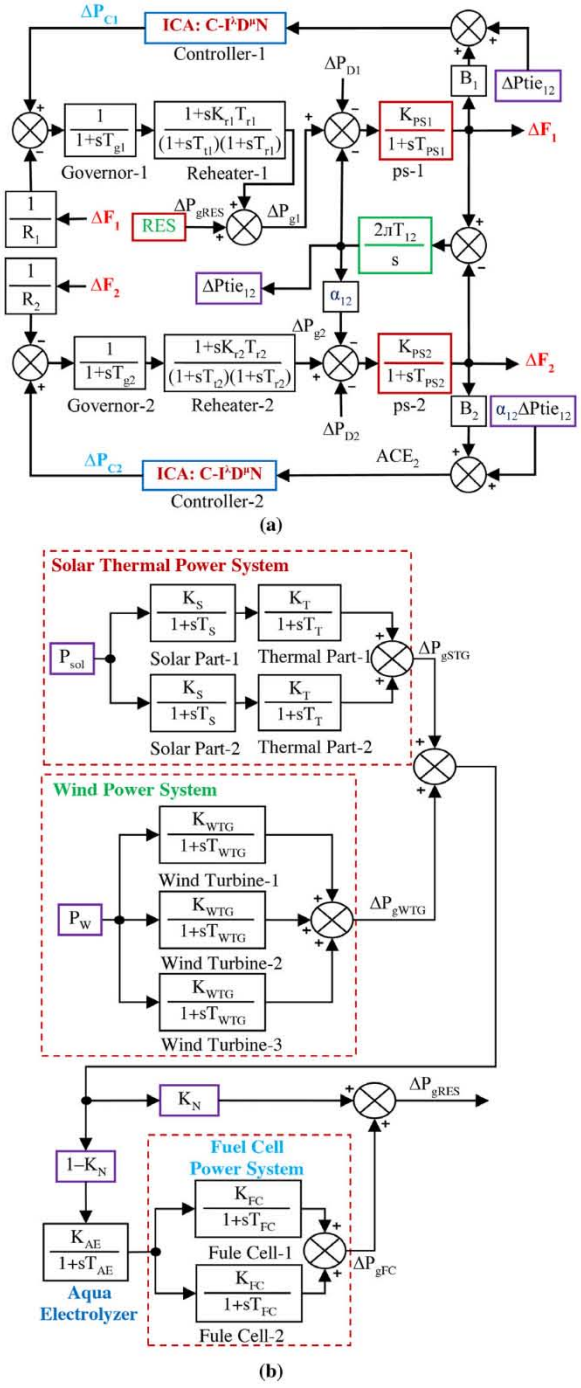

FIGURE 5 (a) 2-area reheat thermal system model [28] and (b) renewable energy sources model [3]

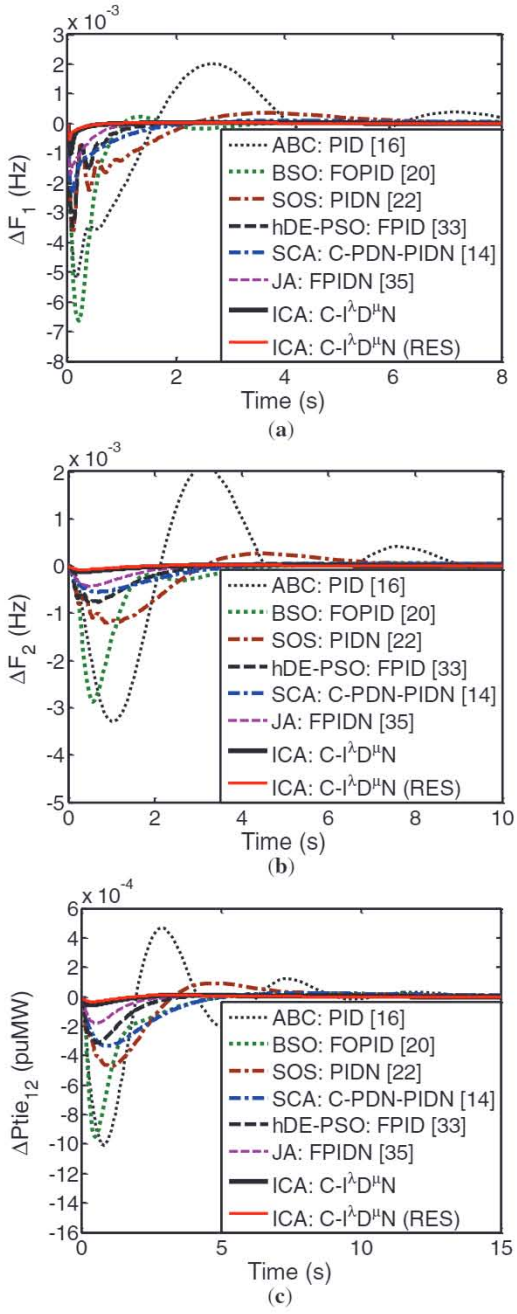

FIGURE 6 2-area reheat thermal system responses (a) ΔF_1, (b) ΔF_2 and (c) $\Delta Ptie_{12}$

3.8 | Convergence

The preceding steps are replicated till the criterion decided for convergence is attained. At the convergence point all empires breakdown except the utmost powerful one. In this condition, all colonies occupy identical positions and costs; competition ends and ICA stops. For more detail please refer [18, 42]. The parameters used in ICA are taken from [29].

4 | OPTIMIZATION CONSTRICTIONS AND OBJECTIVE FUNCTION

To tune the parameters of a controller utilizing an optimization algorithm, an objective/cost function is needed. A cost function (J) is designed based on the desired provisions and limitations. Some of the industry-linked cost functions are integral time absolute error (ITAE), integral square error (ISE), integral time square error (ITSE) and integral absolute error (IAE) [3, 6, 14, 28, 29, 36, 38, 40, 41]. However, in this paper, ISE is utilized because of its better performance [28, 29, 36–38, 40, 41].

TABLE 2 $T_S/U_S/O_S/J_S$ for 2-area reheat thermal system results shown in Figure 6(a–c)

	T_S (s)			U_S (−ve) (Hz)		U_S (−ve) (puMW)	O_S (Hz)		O_S (puMW)	J_S (puMW)			
Controllers	ΔF_1	ΔF_2	$\Delta P\text{tie}_{12}$	ΔF_1	ΔF_2	$\Delta P\text{tie}_{12}$	ΔF_1	ΔF_2	$\Delta P\text{tie}_{12}$	**ISE**	**ITSE**	**IAE**	**ITAE**
ABC: PID [16]	5.39	6.01	1.48	0.0051	0.00329	0.001008	2.01×10^{-3}	2.09×10^{-3}	4.66×10^{-4}	3.62×10^{-5}	5.73×10^{-5}	0.0203	0.0572
SOS: PIDN [22]	1.81	2.29	1.01	0.0036	0.00120	0.000471	3.56×10^{-4}	2.65×10^{-4}	9.15×10^{-5}	6.57×10^{-6}	6.62×10^{-6}	0.0079	0.0203
BSO: FOPID [20]	0.83	1.41	1.05	0.0066	0.00287	0.000949	2.37×10^{-4}	0	0	1.76×10^{-5}	7.36×10^{-6}	0.0078	0.0143
SCA: C-PDN-PIDN [14]	0.95	1.10	0.92	0.0023	0.00054	0.000334	8.92×10^{-5}	4.85×10^{-5}	2.30×10^{-5}	2.05×10^{-6}	1.47×10^{-6}	0.0041	0.0115
hDE-PSO: FPID [33]	0.73	1.24	0.53	0.0034	0.00078	0.000313	0	0	0	2.57×10^{-6}	1.05×10^{-6}	0.0032	0.0062
JA: FPIDN [35]	0.45	0.53	0.52	0.0016	0.00042	0.000180	0	0	0	7.44×10^{-7}	2.62×10^{-7}	0.0015	0.0022
ICA: C-I$^{\lambda}$D$^{\mu}$N	**0.11**	**0.35**	**0.36**	**0.0010**	**0.00013**	**0.000130**	0	0	0	$\mathbf{1.07 \times 10^{-7}}$	$\mathbf{3.32 \times 10^{-8}}$	**0.0006**	**0.0015**
ICA: C-I$^{\lambda}$D$^{\mu}$N (RES)	**0.04**	**0.21**	**0.22**	**0.0005**	**0.00007**	**0.000034**	0	0	0	$\mathbf{3.31 \times 10^{-8}}$	$\mathbf{1.38 \times 10^{-8}}$	**0.0004**	**0.0007**

Bold faces values designate the best values.

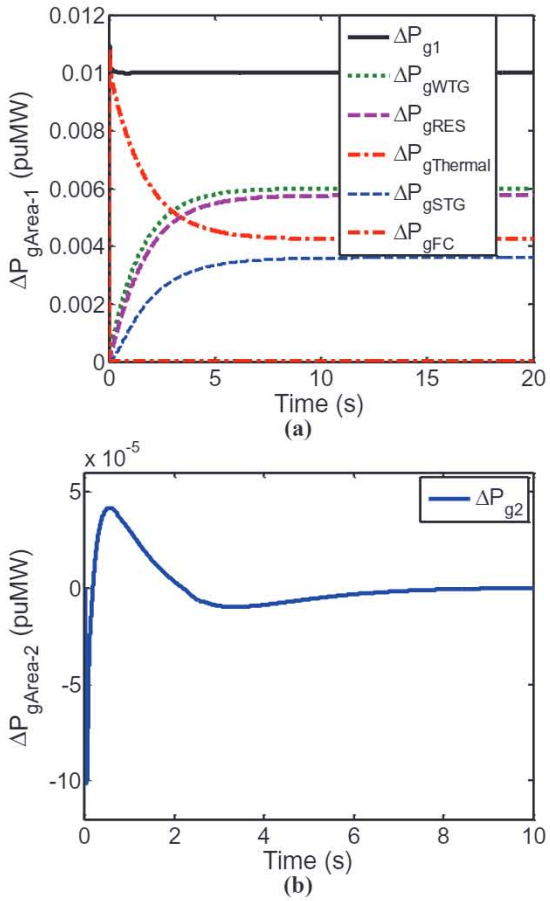

FIGURE 7 2-area reheat thermal system responses (a) $\Delta P_{\text{gArea-1}}$ and (b) $\Delta P_{\text{gArea-2}}$

ISE incorporates the square of the errors over the time, therefore, big errors are penalized more compared to smaller ones. Other performance criteria are utilized to display an effective comparison of the system results. The structure for ISE is given in Equation (17) and other cost functions (J_S) are expressed by Equations (18)–(20).

$$\text{ISE} = \int_0^\infty \left\{\Delta F_1^2 + \Delta F_2^2 + \Delta P\text{tie}_{12}^2\right\} \mathrm{d}t \tag{17}$$

$$\text{ITSE} = \int_0^\infty \text{t}\left\{\Delta F_1^2 + \Delta F_2^2 + \Delta P\text{tie}_{12}^2\right\} \mathrm{d}t \tag{18}$$

$$\text{IAE} = \int_0^\infty \{|\Delta F_1| + \Delta F_2| + |\Delta P\text{tie}_{12}|\} \mathrm{d}t \tag{19}$$

$$\text{ITAE} = \int_0^\infty t\,\{|\Delta F_1| + |\Delta F_2| + |\Delta P\text{tie}_{12}\} \,\mathrm{d}t \tag{20}$$

The results of the systems are attained with the controller parameters acquired for smallest value of Equation (17) using ICA. J_S in Equations (18)–(20) are also computed for comparison purpose. The parameters to be tuned for the proposed C-I$^\lambda$D$^\mu$N controller are 9 ($K_P/K_I/K_D/N/K_{I1}/\lambda/K_{D1}/\mu/N1$) and for outer loop FPIDN are 4 ($K_P/K_I/K_D/N$) parameters. Both controllers are tuned using ICA to get smallest value of (17) in the presence of the following restraints:

$$\left.\begin{array}{l} K_P^{\min} \le K_P \le K_P^{\max} \\ K_I^{\min} \le K_I \le K_I^{\max} \\ K_D^{\min} \le K_D \le K_D^{\max} \\ N^{\min} \le N \le N^{\max} \\ K_{I1}^{\min} \le K_{I1} \le K_{I1}^{\max} \\ \lambda^{\min} \le \lambda \le \lambda^{\max} \\ K_{D1}^{\min} \le K_{D1} \le K_{D1}^{\max} \\ \mu^{\min} \le \mu \le \mu^{\max} \\ N1^{\min} < N1 < \text{N1}^{\max} \end{array}\right\} \tag{21}$$

The min/max in Equation (21) represents minimum/maximum values of the concerned parameter.

TABLE 3 Comparative statistical analysis

Controllers	Minimum	Average	Maximum	SD
C-I$^\lambda$D$^\mu$N	1.07×10^{-7}	4.87×10^{-7}	9.85×10^{-7}	0.17×10^{-7}
C-I$^\lambda$D$^\mu$N (RES)	3.31×10^{-8}	6.43×10^{-8}	9.98×10^{-8}	0.62×10^{-8}

5 | SIMULATION RESULTS

5.1 | Implementation of ICA based control strategy

The models of the systems under examination shown in Figures 5(a) and 8 are designed on MATLAB/SIMULINK platform and ICA programs are prepared in .mfile. The applicable parameters are listed in Appendix. The designed models are simulated in separate programs with/without considering RES for various disturbances in control areas. The objective function is computed in the .m file and utilized in the optimization algorithm. For the execution of ICA, the parameters should be selected carefully as indicated in Section 4. In the present study, no of countries = 500 and number of iteration are taken equal to 100. MATLAB/SIMULINK 7.5.0 (R2007b) is utilized for coding, models and results of the systems. Simulations are performed on an Intel(R), core(TM) i-5-6200U CPU of 2.4 GHz and 8 GB RAM computer. The optimization procedure is reiterated 50 times and the optimum parameters of FPIDN, C-I$^\lambda$D$^\mu$N and C-I$^\lambda$D$^\mu$N (RES) controllers obtained at minimum values of J are provided in Table 1 for 2-area RTS and 2-area MSHTS PS models under study.

5.2 | 2-area reheat thermal system

Primarily, the study is conducted on a more pragmatic 2-area reheat thermal system (RTS) integrated with renewable energy sources (RES) in area-1 (Figure 5(a)). The details of RES are

TABLE 4 T_S, $U_S/O_S/J_S$ for 2-area multi-source hydro-thermal system results shown in Figure 9(a–c)

	T_S (s)			U_S (−ve) (Hz)		U_S (−ve) (puMW)	O_S (Hz)		O_S (puMW)	J_S(puMW)			
Controller type	ΔF_1	ΔF_2	$\Delta Ptie_{12}$	ΔF_1	ΔF_2	$\Delta Ptie_{12}$	ΔF_1	ΔF_2	$\Delta Ptie_{12}$	**ISE**	**ITSE**	**IAE**	**ITAE**
JA-IWO: PID [19]	3.93	4.44	2.25	0.0146	0.0066	0.0027	2.16×10^{-3}	8.00×10^{-4}	2.77×10^{-4}	1.71×10^{-4}	1.26×10^{-4}	0.0311	0.0598
GWO: PID [15]	1.21	3.50	2.64	0.0149	0.0069	0.0026	0	0	0	1.47×10^{-4}	9.03×10^{-5}	0.0233	0.0259
hFA-PS: PID [17]	2.94	4.53	3.30	0.0134	0.0066	0.00220	0	0	0	1.17×10^{-4}	8.50×10^{-5}	0.0255	0.0395
OIO: PID [21]	1.83	3.32	2.06	0.0088	0.0030	0.001000	0	0	0	3.07×10^{-5}	1.80×10^{-5}	0.0132	0.0289
QODSA: PID [24]	1.10	3.36	2.57	0.0154	0.0078	0.002737	2.50×10^{-4}	0	0	1.50×10^{-4}	8.81×10^{-5}	0.0228	0.0255
BFOA: FOPID [38]	1.20	2.15	1.67	0.0115	0.0046	0.0015	4.51×10^{-4}	0	0	5.22×10^{-5}	2.14×10^{-5}	0.0116	0.0121
BFOA: FPI [28]	1.41	2.86	1.92	0.0093	0.0029	0.00108	0	0	0	3.47×10^{-5}	1.76×10^{-5}	0.0122	0.0197
BFOA: FPID [28,38]	0.82	1.79	1.17	0.0065	0.0019	0.00079	2.59×10^{-4}	0	0	1.60×10^{-5}	6.07×10^{-6}	0.0068	0.0083
ICA: FPIDN	0.78	1.59	0.60	0.0047	0.0011	0.00043	0	0	0	6.01×10^{-6}	2.20×10^{-6}	0.0046	0.0082
ICA: C-I$^{\lambda}$D$^{\mu}$N	**0.24**	**0.37**	**0.38**	**0.0027**	**0.0004**	**0.00015**	0	0	0	$\mathbf{9.41 \times 10^{-7}}$	$\mathbf{1.97 \times 10^{-7}}$	**0.0015**	**0.0033**
ICA: C-I$^{\lambda}$D$^{\mu}$N (RES)	**0.18**	**0.21**	**0.27**	**0.0020**	**0.0002**	**0.00009**	0	0	0	$\mathbf{3.68 \times 10^{-7}}$	$\mathbf{5.86 \times 10^{-8}}$	**0.0008**	**0.0013**

Bold faces values designate the best values.

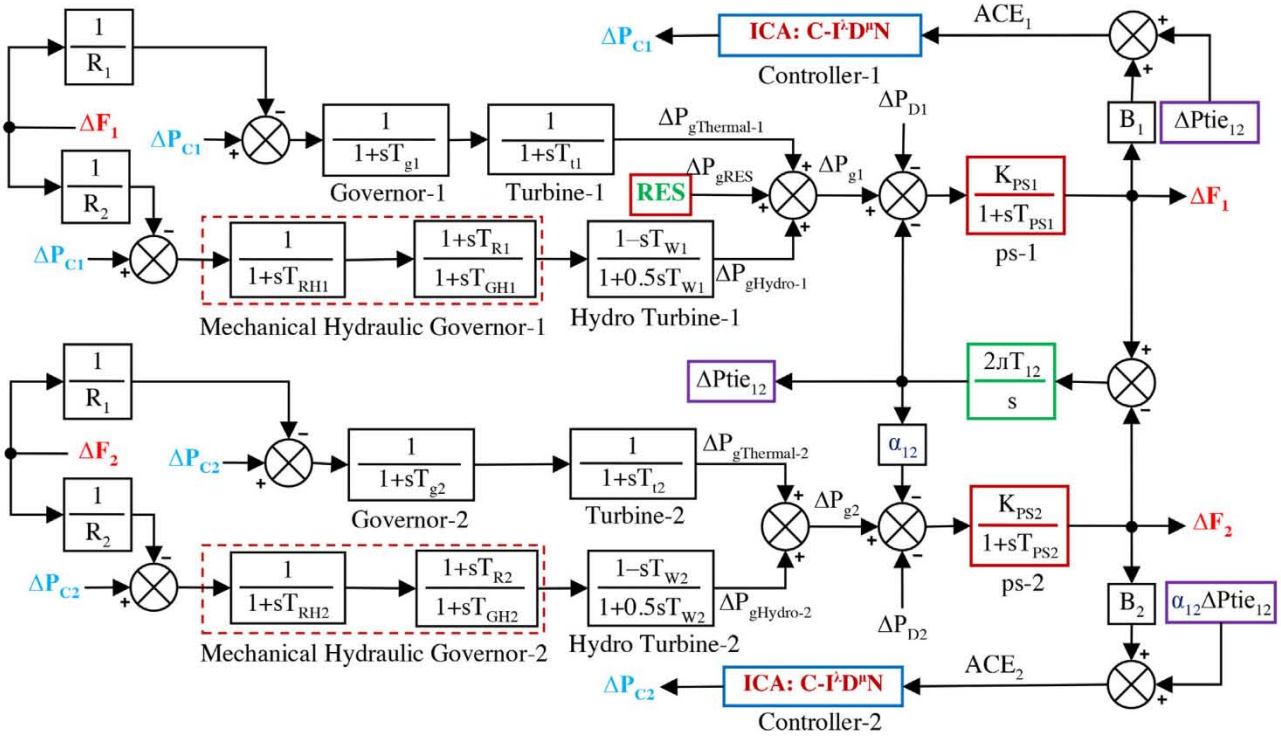

FIGURE 8 2-area multi-source hydro-thermal system model [29]

represented in Figure 5(b). The system dynamic results of change in area-1 frequency (ΔF_1), change in area-2 frequency (ΔF_2) and change in tie power ($\Delta P\text{tie}_{12}$) with the proposed method are obtained by directing a step load perturbation (SLP) of 0.01 puMW in area-1 at time $t = 0$ s. Additionally, a SLP of 0.001 puMW for each STG and 0.002 puMW for each WTG at time $t = 0$ s are considered. The results are exposed in Figure 6(a–c). To reveal the contribution of C-I$^{\lambda}$D$^{\mu}$N controller, its outcomes are matched with various existing and the best claimed intelligent controllers like sine-cosine algorithm (SCA) tuned cascade PDN-PIDN (C-PDN-PIDN) [14], artificial bee colony (ABC) tuned PID [16], bacterial swarm optimization (BSO) tuned fractional order PID (FOPID) [20], SOS algorithm tuned PIDN [22], hybrid differential evolution-PSO (hDE-PSO) tuned FPID [33] and jaya algorithm (JA) tuned FPIDN [35] controllers. The inspection of Figure 6(a–c) divulges that the C-I$^{\lambda}$D$^{\mu}$N controller significantly displays superiority over other controllers in concerning swift responses, no oscillations and negligible settling times (T_S)/peak undershoots (U_S)/overshoots (O_S) in $\Delta F_1/\Delta F_2/\Delta P\text{tie}_{12}$ results.

To inspect the outcome of the C-I$^{\lambda}$D$^{\mu}$N controller further, the numerical values of ISE/ITSE/IAE/ITAE defined via Equations (17)–(20), T_S, U_S and O_S are calculated through simulations and shown in Table 2. Error criteria ISE/ITSE/IAE/ITAE are obtained via simulating the models for 15 s and T_S are obtained for a tolerance band of $\pm$0.0005. Table 2 also demonstrates the advantage of ICA tuned C-I$^{\lambda}$D$^{\mu}$N controller over SCA C-PDN-PIDN [14], ABC PID [16], BSO FOPID [20], SOS PIDN [22], hDE-PSO FPID [33] and JA FPIDN [35] control schemes from least ISE (1.07×10^{-7}), ITSE (3.32×10^{-8}), IAE (0.0006), ITAE (0.0015), T_S ($\Delta F_1 = 0.11$ s, $\Delta F_2 = 0.35$ s, $\Delta P\text{tie}_{12} = 0.36$ s) and U_S ($\Delta F_1 = -0.0010$ Hz, $\Delta F_2 = -0.00013$ Hz, $\Delta P\text{tie}_{12} = -0.000130$ puMW) point of view. Fascinatingly, this observation is not being raised in the corresponding literature that is, in [3] and hence, it establishes a literature gap. It is plainly perceived that C-I$^{\lambda}$D$^{\mu}$N controller is competent in alleviating the oscillations in the system responses. Hence, the disturbance rejection characteristic of C-I$^{\lambda}$D$^{\mu}$N is reasonably appropriate for the AGC compared to other methods.

Further, it is observed that RES comprising of solar thermal generators (STGs), wind turbine generators (WTGs) and aqua electrolyser (AE)-fuel cells (FCs) assist frequency regulation via generating powers in dynamic load condition as indicated in Figure 6(a–c). With C-I$^{\lambda}$D$^{\mu}$N controller in the presence of RES, system performance is observed enriched in terms of further reduction in ISE (3.31×10^{-8}), ITSE (1.38×10^{-8}), IAE (0.0004), ITAE (0.0007), T_S ($\Delta F_1 = 0.04$ s, $\Delta F_2 = 0.21$ s, $\Delta P\text{tie}_{12} = 0.22$ s) and U_S ($\Delta F_1 = -0.0005$ Hz, $\Delta F_2 = -0.00007$ Hz, $\Delta P\text{tie}_{12} = -0.000034$ puMW (Table 2). Next, the generated powers in area-1 ($\Delta P_{\text{gArea-1}}$) and area-2 ($\Delta P_{\text{gArea-2}}$) are shown in Figure 7(a,b). The generated powers by STGs, WTGs, fuel cells (FCs) RES and area-1 thermal are $\Delta P_{\text{gSTG}} = 0.0036$ puMW, $\Delta P_{\text{gWTG}} = 0.006$ puMW, $\Delta P_{\text{gFC}} = 1.536 \times 10^{-7}$puMW, $\Delta P_{\text{gRES}} = 0.00576$ puMW, $\Delta P_{\text{gThermal-1}} = 0.00424$ puMW, respectively. The total power generation in area-1 that is, $\Delta P_{g1} = 0.01$ puMW. Here, ΔP_{g1} ($\Delta P_{\text{gRES}} + \Delta P_{\text{gThermal-1}}$) = ΔP_{D1} that is, generation is equal to

the power demand. However, in area-2, as $\Delta P_{D2} = 0$ puMW, $\Delta P_{gThermal\text{-}2} = \Delta P_{g2} = 0$ puMW.

To check the stability of the proposed ICA based controller, a comparative statistical investigation is performed. The statistical data of minimum, average, maximum and standard deviation (SD) of ISE objective function values achieved in 50 independent runs with the proposed controller (with/without RES) are summarized in Table 3. From the analysis Table 3, it is vibrant that minimum objective function value is attained with the proposed C-I$^{\lambda}$D$^{\mu}$N controller in the presence of RES (ISE = 3.31 $\times 10^{-8}$) compared to C-I$^{\lambda}$D$^{\mu}$N controller (ISE = 1.07 $\times 10^{-7}$). It is also clear from Table 3 that C-I$^{\lambda}$D$^{\mu}$N (RES) outperforms C-I$^{\lambda}$D$^{\mu}$N technique in terms of average, maximum and standard deviation values obtained. It can be stated that the proposed controller is stable and superior specifically with RES for an AGC problem.

5.3 | 2-area multi-source hydro-thermal system

To examine the competence of the C-I$^{\lambda}$D$^{\mu}$N controller to deal with different AGC systems, the study is also widened to a 2-area multi-source hydro-thermal system (MSHTS) whose TF model is displayed in Figure 8. In an area, two units that is, one non-reheat thermal and one mechanical governor outfitted hydro are available. Additionally, RES are integrated in area-1 [3]. The symbols used in the figure are explained in Nomenclature and their values are specified in Appendix. The simulation outcomes of the system at SLP = 0.015 puMW due to the C-I$^{\lambda}$D$^{\mu}$N/fuzzy-PIDN (FPIDN) controllers developed in the study and various other prevalent controllers like grey wolf optimization (GWO) [15]/hFA-PS [17]/JA-IWO [19]/optics inspired optimization (OIO) [21]/quasi oppositional differential search algorithm (QODSA) [24] optimized PID and BFOA optimized FPI/FPID/FOPID [28, 38] are displayed in Figure 9(a–c) and Table 4. It is obvious from Figure 9(a–c) and Table 4 that the offered controller parades improved dynamic outcome in contrast to the published controllers and ICA tuned FPIDN controller. It is perceived that lowest values of ISE (9.41 $\times 10^{-7}$), ITSE (1.97 $\times 10^{-7}$), IAE (0.0015), ITAE (0.0033), T_S (ΔF_1 = 0.24 s, ΔF_2 = 0.37 s, ΔPtie$_{12}$ = 0.38 s) and U_S (ΔF_1 = −0.0027 Hz, ΔF_2 = −0.0004 Hz, ΔPtie$_{12}$ = −0.00015 puMW) are obtained with C-I$^{\lambda}$D$^{\mu}$N controller compared to ICA based FPIDN controller which provides somewhat greater values of ISE (= 6.01 $\times 10^{-6}$) ITSE (= 2.20 $\times 10^{-6}$), IAE (= 0.0046), ITAE (= 0.0082), T_S (ΔF_1 = 0.78 s, ΔF_2 = 1.59 s, ΔPtie$_{12}$ = 0.60 s) and U_S (ΔF_1 = −0.0047 Hz, ΔF_2 = −0.0011 Hz, ΔPtie$_{12}$ = −0.00043 puMW). It should be noted that ICA based FPIDN controller offers better results than JA-IWO [19]/QODSA [24]/GWO [15]/hFA-PS [17]/OIO [21] based PID and BFOA based FPI/FPID/FOPID [28, 38] controllers. However, performance of the recommended C-I$^{\lambda}$D$^{\mu}$N controller is additionally advanced in the company of RES as clearly indicated in Figure 9(a–c) and Table 4.

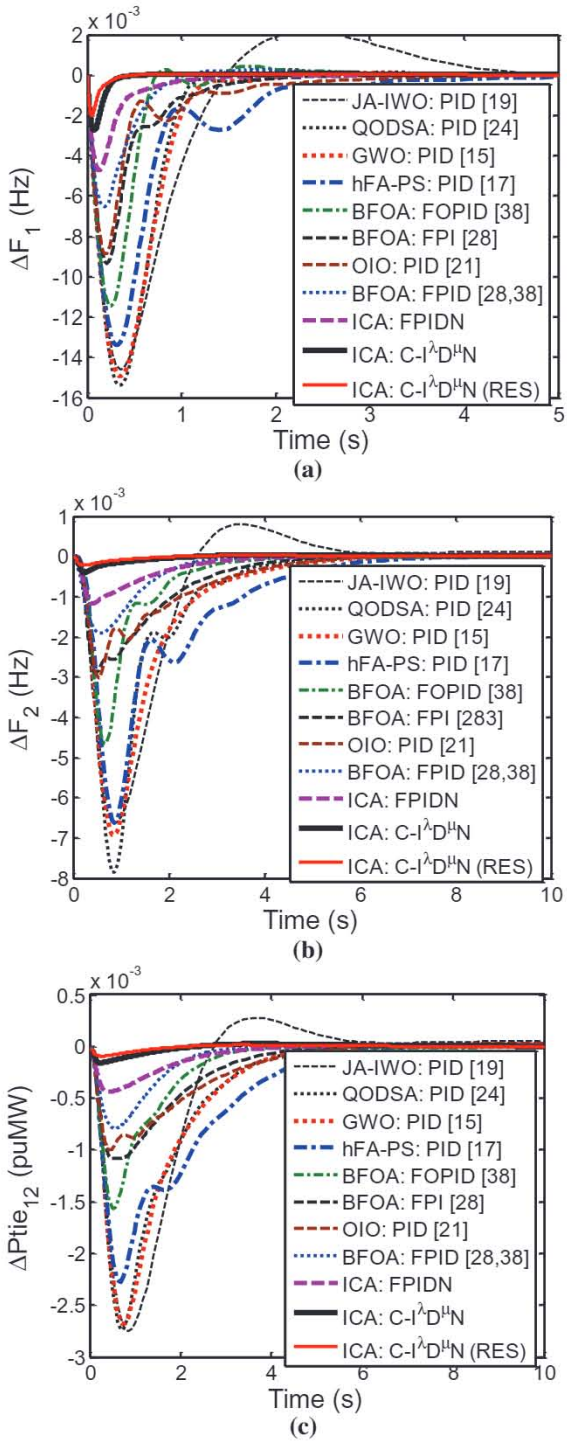

FIGURE 9 2-area multi-source hydro-thermal system responses: (a) ΔF_1, (b) ΔF_2 and (c) ΔPtie$_{12}$

The generation results in area-1 ($\Delta P_{gArea\text{-}1}$) and area-2 ($\Delta P_{gArea\text{-}2}$) are exposed in Figure 10(a,b). The generated powers by STGs, WTGs, FCs, RES, area-1 thermal and area-1 hydro are ΔP_{gSTG} = 0.0036 puMW, ΔP_{gWTG} = 0.006 puMW, ΔP_{gFC} = 1.536 $\times 10^{-7}$ puMW, ΔP_{gRES} = 0.00576 puMW, $\Delta P_{gThermal\text{-}1}$ = 0.004622 puMW, $\Delta P_{gHydro\text{-}1}$ = 0.004618 puMW,

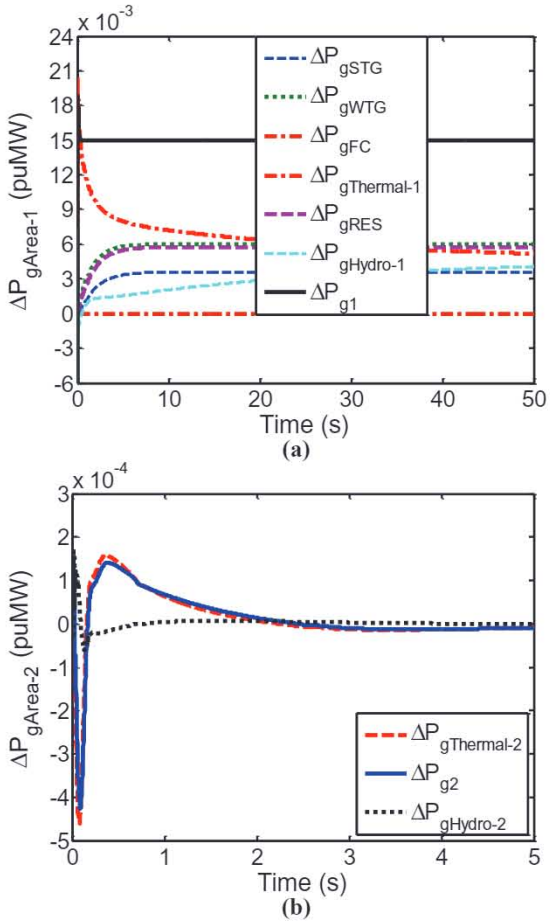

FIGURE 10 2-area multi-source hydro-thermal system responses: (a) $\Delta P_{\text{gArea-1}}$ and (b) $\Delta P_{\text{gArea-2}}$

respectively. The total power generation in area-1 that is, ΔP_{g1} $(= \Delta P_{\text{gRES}} + \Delta P_{\text{gThermal-1}} + \Delta P_{\text{gHydro-1}}) = 0.015$ puMW, which is equal to the demand in area-1 that is, ΔP_{D1}. However, in area-2, as $\Delta P_{D2} = 0$ puMW, $\Delta P_{\text{gThermal-2}} = 0$ puMW, $\Delta P_{\text{gHydro-2}} = 0$ puMW and $\Delta P_{g2} = (\Delta P_{\text{gThermal-2}} + \Delta P_{\text{gHydro-2}}) = 0$ puMW.

Next, in practical scenario, the power outputs of STG and WTG renewable sources are highly unpredictable and variable due to their dependence on environmental factors like solar irradiation and wind speed. Consequently, the deviations in their power outputs are inspected in the existence of random powers (P_{sol}) and (P_{W}) caused due to solar insolation and wind speed respectively varying abruptly with time as shown in Figure 11(a). However, SLP in area-1 remains the same. With the proposed controller, the simulation results of generations in area-1 that is ΔP_{gSTG}, ΔP_{gWTG}, ΔP_{gFC}, ΔP_{gRES}, $\Delta P_{\text{gThermal-1}}$, $\Delta P_{\text{gHydro-1}}$ and ΔP_{g1} are shown in Figure 11(b). It is observed from Figure 11(b) that the generations are changing randomly in contrast to Figure 10(a). However, in steady state, ΔP_{g1} fluctuates around the required 0.015 puMW ($= \Delta P_{D1}$) power. The simulation results of generations in area-2 shown in Figure 11(c) fluctuates around zero as $\Delta P_{D2} = 0$ puMW, which satisfies the AGC requirement effectively. It is observed that the proposed controller works efficiently in this realistic

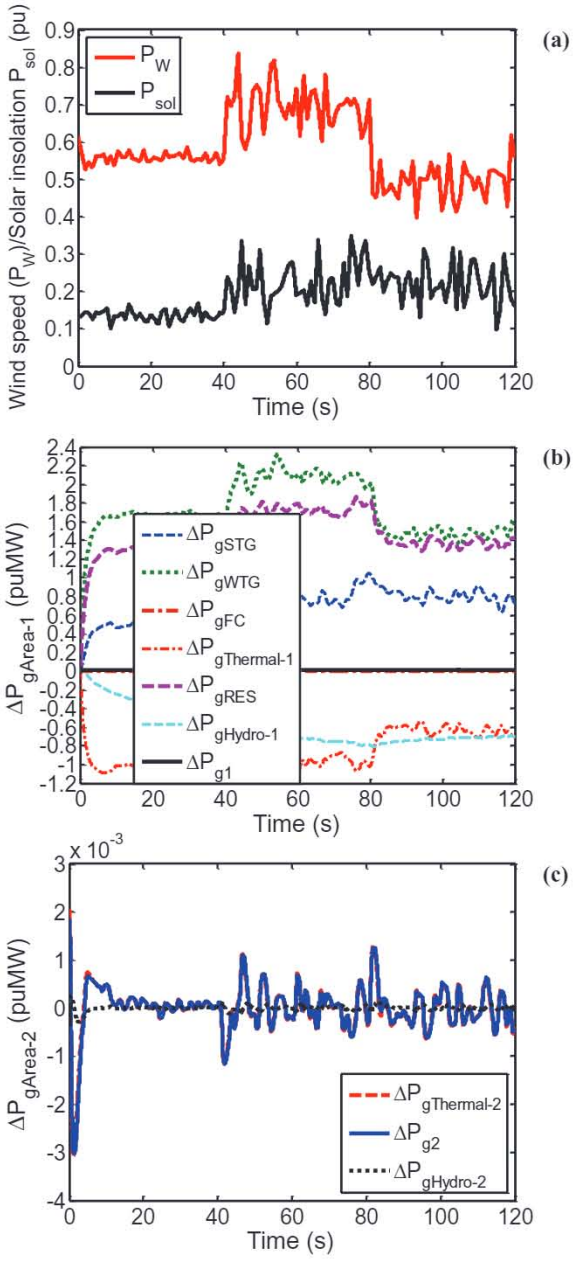

FIGURE 11 2-area multi-source hydro-thermal system responses under abrupt $P_{\text{sol}}/P_{\text{W}}$: (a) $P_{\text{sol}}/P_{\text{W}}$, (b) $\Delta P_{\text{gArea-1}}$ and (c) $\Delta P_{\text{gArea-2}}$

circumstance. However, J_S values increases from the values shown in Table 4 (ISE = 3.68×10^{-7}, ITSE = 5.86×10^{-8}, IAE = 0.0008 and ITAE = 0.0013) due to longer simulation time and abrupt/higher disturbances taking place in the form of $P_{\text{sol}}/P_{\text{W}}$ power as: ISE = 3.93×10^{-4}, ITSE = 1.27×10^{-2}, IAE = 0.2072 and ITAE = 11.32.

6 | SENSITIVITY STUDY

A sensitivity study is performed to check the robustness of the recommended C-I$^{\lambda}$D$^{\mu}$N controller for extensive deviations in the system operating conditions. To illustrate the robustness,

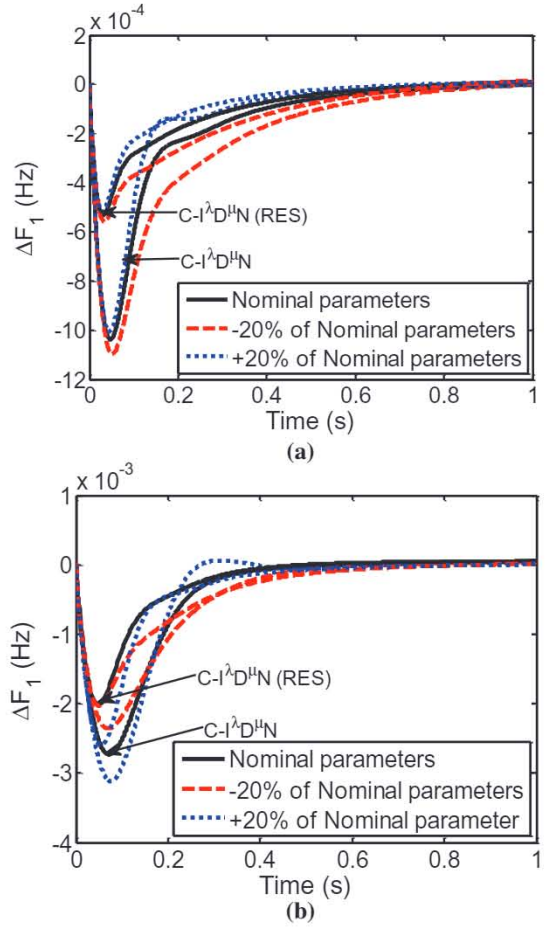

FIGURE 12 Sensitivity study responses: (a) ΔF_1 of reheat thermal system and (b) ΔF_1 of multi-source hydro-thermal system

system's nominal parameters stated in Appendix are altered for ±20%. The C-I$^{\lambda}$D$^{\mu}$N controller should behave healthy devoid of considerable deterioration in the system's results under parameter deviations. Figure 12(a,b) demonstrates ΔF_1 results under nominal and ±20% variations in parameters for 2-area reheat thermal system and multi-source hydro-thermal system, in order with/without RES. Here, ΔF_2 and $\Delta P\text{tie}_{12}$ responses are not provided to save the space. The inspection of Figure 12(a,b) evidently reveals that all results with/without RES are stable and they do not deviate much from the nominal responses. However, controller outperforms in the continuation of RES. The several performance indices that is, T_S and J_S for nominal parameters and ±20% of nominal parameter variation cases for reheat thermal system (with/without RES) and multi-source hydro-thermal system (with/without RES) are given in Table 5 for ΔF_1, ΔF_2 and $\Delta P\text{tie}_{12}$ responses. It can be perceived from Table 5 that settling time, ISE, ITSE, IAE and ITAE values diverge within tolerable ranges and are more or less equal to the corresponding values attained with nominal system parameters. Therefore, it can be established that the proposed controller is robust and executes suitably when system nominal parameters deviate in the range ±20%.

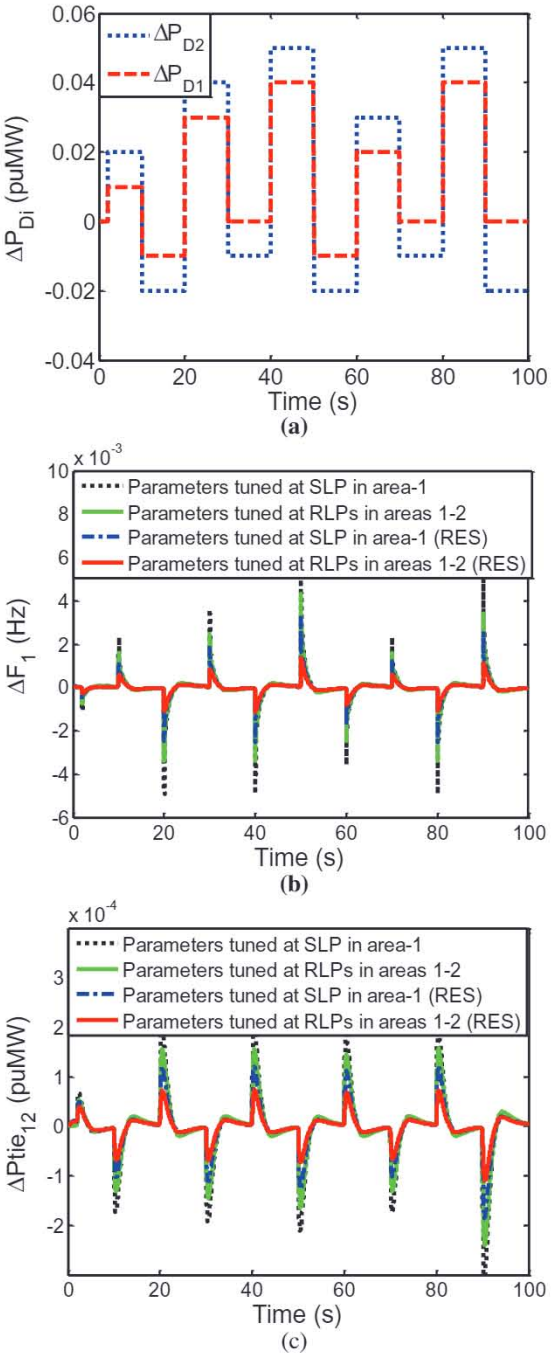

FIGURE 13 Responses of reheat thermal system during sensitivity study (a) RLPs in areas 1–2, (b) ΔF_1 and (c) $\Delta P\text{tie}_{12}$

Additionally, the robustness study of the C-I$^{\lambda}$D$^{\mu}$N controller is performed out under the existence of random load perturbations (RLPs) of high magnitudes in both control areas of 2-area reheat thermal system. Dissimilar RLPs in all control areas represent a much more realistic power system environment. At higher SLP/RLP scenario, the power system will become unbalanced if the designed controller is non-robust. Figure 13(a) shows RLPs of different magnitudes applied in areas 1 and 2 at t = 2 s of reheat thermal system. Figure 13(b,c) show ΔF_1 and $\Delta P\text{tie}_{12}$ responses with parameters of the C-I$^{\lambda}$D$^{\mu}$N

TABLE 5 Sensitivity study data for T_S and J_S

Parameter variations	ΔF_1 (Hz)	ΔF_2 (Hz)	$\Delta Ptie_{12}$ (puMW)	ISE	ITSE	IAE	ITAE
Reheat thermal system (C-I$^{\lambda}$D$^{\mu}$N) (Figure 12(a))							
Nominal parameters	0.11	0.35	0.36	1.07×10^{-7}	3.32×10^{-8}	0.0006	0.0015
−20% of Nominal parameters	0.12	0.36	0.37	1.66×10^{-7}	5.97×10^{-8}	0.0008	0.0018
+20% of Nominal parameters	0.10	0.34	0.35	0.11×10^{-7}	2.64×10^{-8}	0.0005	0.0014
Reheat thermal system (C-I$^{\lambda}$D$^{\mu}$N (RES) (Figure 12(a))							
Nominal parameters	0.04	0.21	0.22	3.31×10^{-8}	1.38×10^{-8}	0.0004	0.0007
−20% of Nominal parameters	0.05	0.22	0.23	5.53×10^{-8}	3.08×10^{-8}	0.0005	0.0010
+20% of Nominal parameters	0.05	0.20	0.21	2.33×10^{-8}	7.16×10^{-9}	0.0003	0.0005
Multi-source hydro-thermal system (C-I$^{\lambda}$D$^{\mu}$N) (Figure 12(b))							
Nominal parameters	0.24	0.37	0.38	9.41×10^{-7}	1.97×10^{-7}	0.0015	0.0033
−20% of Nominal parameters	0.27	0.39	0.40	8.42×10^{-7}	2.45×10^{-7}	0.0017	0.0038
+20% of Nominal parameters	0.21	0.33	0.34	1.13×10^{-6}	1.90×10^{-7}	0.0014	0.0028
Multi-source hydro-thermal system (C-I$^{\lambda}$D$^{\mu}$N (RES) (Figure 12(b))							
Nominal parameters	0.18	0.21	0.27	3.68×10^{-7}	5.86×10^{-8}	0.0008	0.0013
−20% of Nominal parameters	0.20	0.23	0.28	5.30×10^{-7}	1.10×10^{-7}	0.0011	0.0015
+20% of Nominal parameters	0.18	0.20	0.26	6.14×10^{-7}	9.03×10^{-8}	0.0009	0.0011

controller optimized at area-1 SLP of 0.01 puMW (given in Table 1) and RLPs in areas 1–2. The optimized controller parameters obtained at this SLP produce ISE = 9.47×10^{-5}/ITSE = 5.10×10^{-3}/IAE = 0.0551/ITAE = 2.8890 and ISE = 3.26×10^{-5}/ITSE = 1.76×10^{-3}/IAE = 0.0372/ITAE = 1.9520 (with RES), which are greater than their corresponding values given in Table 2. This means that the controller with RES produces better performance regarding J_S and results shown in Figure 13(b,c). Next, the optimized controller parameters obtained at RLPs are K_P = 4.8589, K_I = 4.6874, K_D = 0.1499, N = 460.4499, K_{I1} = 4.5624, λ = 0.3401, K_{D1} = 0.8031, μ = 0.4089 and $N1$ = 489.0021 and K_P = 4.5682, K_I = 4.9984, K_D = 0.4681, N = 447.8967, K_{I1} = 4.9564, λ = 0.2499, K_{D1} = 0.9785, μ = 0.4934 and $N1$ = 467.7896 (with RES). The J_S results are ISE = 5.57×10^{-5}/ITSE = 3.01×10^{-3}/IAE = 0.0501/ITAE = 2.6360 and ISE = 1.46×10^{-5}/ITSE = 7.87×10^{-4}/IAE = 0.0295/ITAE = 1.5470 (RES). Serious inspection of Figure 13(c) evidently discloses that both the responses are stable. However, system responses and J_S obtained at parameters optimized with RLPs are superior. Thus, the stable performance of the system at dissimilar operating conditions authorizes the robustness of ICA optimized C-I$^{\lambda}$D$^{\mu}$N controller.

7 | CONCLUSION

A novel ICA tuned C-I$^{\lambda}$D$^{\mu}$N controller is suggested for AGC of 2-area electric PSs penetrated with RES. Initially, a 2-area RTS is scrutinized in the presence of 1% SLP in control area-1. The simulation results due to the proposed controller are compared with the existing ABC tuned PID, BSO tuned FOPID, SOS tuned PIDN, hDE-PSO tuned FPID and JA tuned FPIDN controllers. It is noted that significant development regarding oscillation free results with smallest values of $T_S/U_S/O_S/J_S$ are obtained due to the suggested ICA tuned C-I$^{\lambda}$D$^{\mu}$N controller over other controllers. However, further enhanced results are acquired in the presence of RES integrated in area-1. To further validate the capability, extensibility and advantage of the method for other systems, the work is also protracted to a 2-area MSHTS. The asset of C-I$^{\lambda}$D$^{\mu}$N controller is established over ICA based FPIDN and intelligent JA- IWO/QODSA/GWO/hFA-PS/OIO tuned PID and BFOA tuned FPI/FPID/FOPID controllers prevailing in the literature. The worth of RES addition is validated via enhanced system outcome with the C-I$^{\lambda}$D$^{\mu}$N controller. The sensitivity analysis validates the robustness of the C-I$^{\lambda}$D$^{\mu}$N controller with/without RES under ±20% deviations in the system's parameters and random load perturbations (RLPs) created in both areas of reheat thermal system. It is observed that the proposed controller designed at nominal condition is robust and shows stable performance at extensive changes in the parameters of the systems and RLPs. Additionally, RES integration is suggested in PSs to get reliable, better quality, and environmentally-friendly electrical power.

Hence, after analysis and discussion done above, it is assured that the suggested ICA optimized C-I$^{\lambda}$D$^{\mu}$N controller may be an appropriate controller for solving more intricate engineering problems in isolated/multi-area interconnected traditional as well as modern restructured AGC systems with/without RES integration.

Nomenclature

B	frequency bias constant, puMW/Hz
K_{AE}	aqua electrolyser gain
K_{FC}	fuel cell gain
K_{PS}	power system gain
K_r	reheater gain
K_S, K_T	solar thermal generator gains
K_{WTG}	wind turbine generator gain
R	speed governor regulation parameter, Hz/puMW
T_{12}	synchronizing coefficient of tie-line, puMW/rad
T_{AE}	aqua electrolyser time constant (TC), s
T_{FC}	fuel cell time constant, s
T_g	thermal governor TC, s
T_{GH}	hydro governor main servo TC, s
T_{PS}	power system time constant (TC), s
T_r	reheater TC, s
T_R	hydro governor reset time, s
T_{RH}	time constant of hydro governor transient droop, s
T_S, T_T	solar thermal generator TCs, s
T_t	thermal turbine TC, s
T_W	water starting time, s
T_{WTG}	wind turbine generator TC, s
α_{12}	area rating ratio

ORCID

Yogendra Arya https://orcid.org/0000-0003-4661-1950
Nishant Kumar https://orcid.org/0000-0003-4084-7436
Pankaj Dahiya https://orcid.org/0000-0002-2722-1554
Gulshan Sharma https://orcid.org/0000-0002-4726-0956
Emre Çelik https://orcid.org/0000-0002-2961-0035
Sandeep Dhundhara https://orcid.org/0000-0003-4403-4897
Mandeep Sharma https://orcid.org/0000-0002-7217-1410

REFERENCES

1. Nanda, J., et al.: A new technique in hydro thermal interconnected automatic generation control system by using minority charge carrier inspired algorithm. Int. J. Elect. Power Energy Syst. 68, 259–268 (2015)
2. Rahman, A., et al.: AGC of dish-Stirling solar thermal integrated thermal system with biogeography based optimised three degree of freedom PID controller. IET Renew. Power Gener. 10(8), 1161–1170 (2016)
3. Kler, D., et al.: Optimal integral minus proportional derivative controller design by evolutionary algorithm for thermal-renewable energy-hybrid power systems. IET Renewab. Power Gener. 13(11), 2000–2012 (2019)
4. Das, D.C., Roy, A.K., Sinha, N.: GA based frequency controller for solar thermal-diesel-wind hybrid energy generation/energy storage system. Int. J. Elect. Power Energy Syst. 43(1), 262–279 (2012)
5. Arya Y.: Impact of hydrogen aqua electrolyzer-fuel cell units on automatic generation control of power systems with a new optimal fuzzy TIDF-II controller. Renewab. Energy 139, 468–482 (2019)
6. Tasnin, W., et al.: Deregulated AGC of multi-area system incorporating dish-stirling solar thermal and geothermal power plants using fractional order cascade controller. Int. J. Elect. Power Energy Syst. 101, 60–74 (2018)
7. Tasnin, W., Saikia, L.C.: Maiden application of an sine-cosine algorithm optimised FO cascade controller in automatic generation control of multi-area thermal system incorporating dish-stirling solar and geothermal power plants. IET Renewab. Power Gener. 12(5), 585–597 (2018)
8. Xi, L., et al.: Wolf pack hunting strategy for automatic generation control of an islanding smart distribution network. Energy Convers. Manage. 122, 10–24 (2016)
9. Xi, L., et al.: A novel multi-agent DDQN-AD method-based distributed strategy for automatic generation control of integrated energy systems. IEEE Trans. Sustainab. Energy 11 (2020) https://doi.org/10.1109/TSTE.2019.2958361.
10. Xi, L. et al.: A deep reinforcement learning algorithm for the order optimization allocation of total power in the interconnected power grids. CSEE J. Power Energy Syst., 2020, https://doi.org/10.17775/CSEEJPES.2019.01840.
11. Xi, L., et al.: A virtual generation ecosystem control strategy for automatic generation control of interconnected microgrids. IEEE Access 8, 94165–94175 (2020)
12. Xi, L., et al.: Smart generation control based on multi-agent reinforcement learning with the idea of the time tunnel. Energy 153, 977–987 (2018)
13. Xi, L., et al.: Automatic generation control based on multiple neural networks with actor-critic strategy. IEEE Trans. Neural Net. Learning Syst. (2020), https://doi.org/10.1109/TNNLS.2020.3006080.
14. Satapathy, P., et al.: Design of PD-PID controller with double derivative filter for frequency regulation. In 2nd IEEE International Conference on Power Electronics, Intelligent Control and Energy Systems, Delhi, India, 2018, pp. 1142–1147 (2018)
15. Guha, D., et al.: Load frequency control of interconnected power system using grey wolf optimization. Swarm Evol. Comput. 27, 97–115 (2016)
16. Gozde, H., et al.: Comparative performance analysis of artificial bee colony algorithm in automatic generation control for interconnected reheat thermal power system. Int. J. Elect. Power Energy Syst. 42(1), 167–178 (2012)
17. Sahu, R.K., et al.: A hybrid firefly algorithm and pattern search technique for automatic generation control of multi area power systems. Int. J. Elect. Power Energy Syst. 64, 9–23 (2015)
18. Shabani, H., et al.: A robust PID controller based on imperialist competitive algorithm for load-frequency control of power systems. ISA Trans. 52(1), 88–95 (2013)
19. Oozeer, M.Y., Ramjug-Ballgobin, R.: A jaya-based invasive weed optimization technique for load frequency control. In: Fleming P, Lacquet B, Sanei S, Deb K, Jakobsson A. (eds.) Smart and Sustainable Engineering for Next Generation Applications. ELECOM 2018, Lecture Notes Elect Eng, vol. 561, pp. 11–21 Springer, Singapore (2019)
20. Ozdemir, M.T., et al: Tuning of optimal classical and fractional order PID parameters for automatic generation control based on the bacterial swarm optimization. IFAC-PapersOnLine 48(30), 501–506 (2015)
21. Ozdemir, M.T., Ozturk, D.: Comparative performance analysis of optimal PID parameters tuning based on the optics inspired optimization methods for automatic generation control. Energies 10(12), 2134.
22. Hasanien, H.M., El-Fergany, A.: Symbiotic organisms search algorithm for automatic generation control of interconnected power systems including wind farms. IET Gener. Transm. Distrib. 11(7), 1692–1700 (2017)
23. Guha, D., et al.: Symbiotic organism search algorithm applied to load frequency control of multi-area power system. Energy Syst. 9(2), 439–468 (2018)
24. Guha, D., et al.: Quasi-oppositional differential search algorithm applied to load frequency control. Eng. Sc. Tech. an Int. J. 19(4), 1635–1654 (2016)
25. Manoharan, N., et al.: Automatic generation control by hybrid invasive weed optimization and pattern search tuned 2-DOF PID controller. Int. J. Comput. Communicat. Contr. 12(4), 533–549 (2017)
26. Saha, A., Saikia, L.C.: Utilisation of ultra-capacitor in load frequency control under restructured STPP-thermal power systems using WOA optimised PIDN-FOPD controller. IET Gener. Transm. Distrib. 11(13), 3318–3331 (2017)
27. Sahu, R.K., et al.: A novel hybrid PSO-PS optimized fuzzy PI controller for AGC in multi area interconnected power systems. Int. J. Elect. Power Energy Syst. 64, 880–893 (2015)
28. Arya, Y., Kumar, N.: Design and analysis of BFOA-optimized fuzzy PI/PID controller for AGC of multi-area traditional/restructured electrical power systems. Soft Comput. 21(21), 6435–6452 (2017)
29. Arya, Y.: Automatic generation control of two-area electrical power systems via optimal fuzzy classical controller. J. Franklin Inst. 355(5), 2662–2688 (2018)

30. Barisal, A.K., et al.: A hybrid PSO-levy flight algorithm based fuzzy PID controller for automatic generation control of multi area power systems: fuzzy based hybrid PSO for automatic generation control. Int. J. Energy Optimizat. Eng. 6(2), 42–63 (2017)
31. Gheisarnejad, M.: An effective hybrid harmony search and cuckoo optimization algorithm based fuzzy PID controller for load frequency control. Appl. Soft. Comput. 65, 121–138 (2018)
32. Rajesh, K.S., et al.: Hybrid improved firefly-pattern search optimized fuzzy aided PID controller for automatic generation control of power systems with multi-type generations. Swarm Evol. Comput. 44, 200–211 (2019)
33. Sahu, B.K., et al.: Hybrid differential evolution particle swarm optimisation optimised fuzzy proportional-integral derivative controller for automatic generation control of interconnected power system. IET Gener. Transm. Distrib. 8(11), 1789–1800 (2014)
34. Mohanty, P.K., et al: Design and analysis of fuzzy PID controller with derivative filter for AGC in multi-area interconnected power system. IET Gener. Transm. Distrib. 10(15), 3764–3776 (2016)
35. Debnath, M.K., et al.: Application of fuzzy-PIDF controller for automatic generation control using jaya algorithm. Int. J. Pure Appl. Math. 114(9), 51–61 (2017)
36. Arya, Y.: AGC performance enrichment of multi-source hydrothermal gas power systems using new optimized FOFPID controller and redox flow batteries. Energy 127, 704–715 (2017)
37. Arya, Y.: AGC of restructured multi-area multi-source hydrothermal power systems incorporating energy storage units via optimal fractional-order fuzzy PID controller. Neural Comput. Appl. 31(3), 851–872 (2019)
38. Arya, Y., Kumar N.: BFOA-scaled fractional order fuzzy PID controller applied to AGC of multi-area multi-source electric power generating systems. Swarm Evol. Comput. 32, 202–218 (2017)
39. Mahto, T., Mukherjee, V.: Fractional order fuzzy PID controller for wind energy-based hybrid power system using quasi-oppositional harmony search algorithm. IET Gener. Transm. Distrib. 11(13), 3299–3309 (2017)
40. Arya, Y.: A new optimized fuzzy FOPI-FOPD controller for automatic generation control of electric power systems. J. Franklin Inst. 356(11), 5611–5629 (2019)
41. Arya, Y.: A novel CFFOPI-FOPID controller for AGC performance enhancement of single and multi-area electric power systems. ISA Trans. 100, 126–135 (2019), https://doi.org/10.1016/j.isatra.2019.11.025.
42. Atashpaz-Gargari, E., Lucas, C.: Imperialist competitive algorithm: an algorithm for optimization inspires by imperialistic competition. In: IEEE Congress on Evolutionary Computation, Singapore, 2007, pp. 4661–4667 (2007).

How to cite this article: Arya Y, Kumar N, Dahiya P, et al. Cascade-$I^{\lambda}D^{\mu}N$ controller design for AGC of thermal and hydro-thermal power systems integrated with renewable energy sources. *IET Renew Power Gener.* 2021;15:504–520. https://doi.org/10.1049/rpg2.12061

APPENDIX: SYSTEM DATA

2-area reheat thermal system (RTS) [16]:

P_{ri} = 2000 MW, T_{PSi} = 20 s, K_{PSi} = 120 Hz/puMW, T_{gi} = 0.08 s, T_{ti} = 0.3 s, K_{ri} = 0.5, T_{ri} = 10 s, $2\pi T_{12}$ = 0.545 puMW/Hz, B_i = 0.425 puMW/Hz, R_i = 2.4 Hz/puMW, $\alpha_{12} = -1$, F^0 = 60 Hz, initial loading = 50%.

2-area multi-source hydro-thermal system (MSHTS) [17]:

P_{ri} = 2000 MW, T_{PSi} = 20 s, K_{PSi} = 100 Hz/puMW, T_{ti} = 0.3 s, T_{gi} = 0.08 s, R_2 = 2.4 Hz/puMW, T_{12} = 0.0707 puMW/rad, B_i = 0.425 puMW Hz < sp > -1 < ,/sp > T_{Ri} = 5 s, T_{RHi} = 48.7 s, T_{Wi} = 1 s, T_{GHi} = 0.513 s, R_1 = 2 Hz/puMW, $\alpha_{12} = -1$, F^0 = 60 Hz, initial loading = 50%.

Renewable energy sources (RES) [3]:

K_S = 1.8, T_S = 1.8 s, K_T = 1, T_T = 0.3 s, K_{WTG} = 1, T_{WTG} = 1.5 s, K_N = 0.6, K_{AE} = 0.002, T_{AE} = 0.5 s, K_{FC} = 0.01, T_{FC} = 4 s.